Acceleration of Tissue Plasminogen Activator Mediated Thrombolysis by Magnetically Powered Nanomotors

Rui Cheng [1], Weijie Huang [2*], Lijie Huang [3,4], Bo Yang[5], Leidong Mao [1], Kunlin Jin [3], Qichuan ZhuGe[4], and Yiping Zhao[2**]*

[1]College of Engineering, Nanoscale Science and Engineering Center, University of Georgia, Athens, Georgia 30602, USA

[2]Department of Physics and Astronomy, Nanoscale Science and Engineering Center, University of Georgia, Athens, Georgia 30602, USA

[3]Department of Pharmacology and Neuroscience, Institute for Alzheimer's Disease and Aging Research, University of North Texas Health Science Center, Fort Worth, Texas 76107, USA

[4] Zhejiang Provincial Key Laboratory of Aging and Neurological Disorder Research, The First Affiliated Hospital of Wenzhou Medical University, Wenzhou, Zhejiang, 325000, China

[5] Department of Mechanical and Aerospace Engineering, University of Texas, Arlington, TX 76019, USA

Supplementary Information

1. Experimental information

1.1 In-vitro experimental setup

As shown in **Figure S1(a),** the experimental setup consists of a magnetic field generator, a PDMS plate with test samples inside, a light pad, and a data acquisition system. Particularly, the rotating magnetic field is generated by four solenoids (Air-core Solenoid #14825, Science Source, Waldoboro, ME), which are connected to two independent power supplies and controlled by a computer. The PDMS plate is suspended at the center of the solenoids by a glass slide with printed scales (green-dash lines), and is placed above a light pad (LightPad A920, Artograph, Delano, MN) which can provide a uniform and stable white light illumination for

* Equal contribution

** Corresponding author, email: zhaoy@physast.uga.edu, telephone: 1-706-542-7792, fax: 1-706-542-2492.

quantitative data extraction. The experimental data are obtained by a digital camera (Infinity 1, Lumenera Corp, Ottawa, Canada) monitoring PDMS channel from the top.

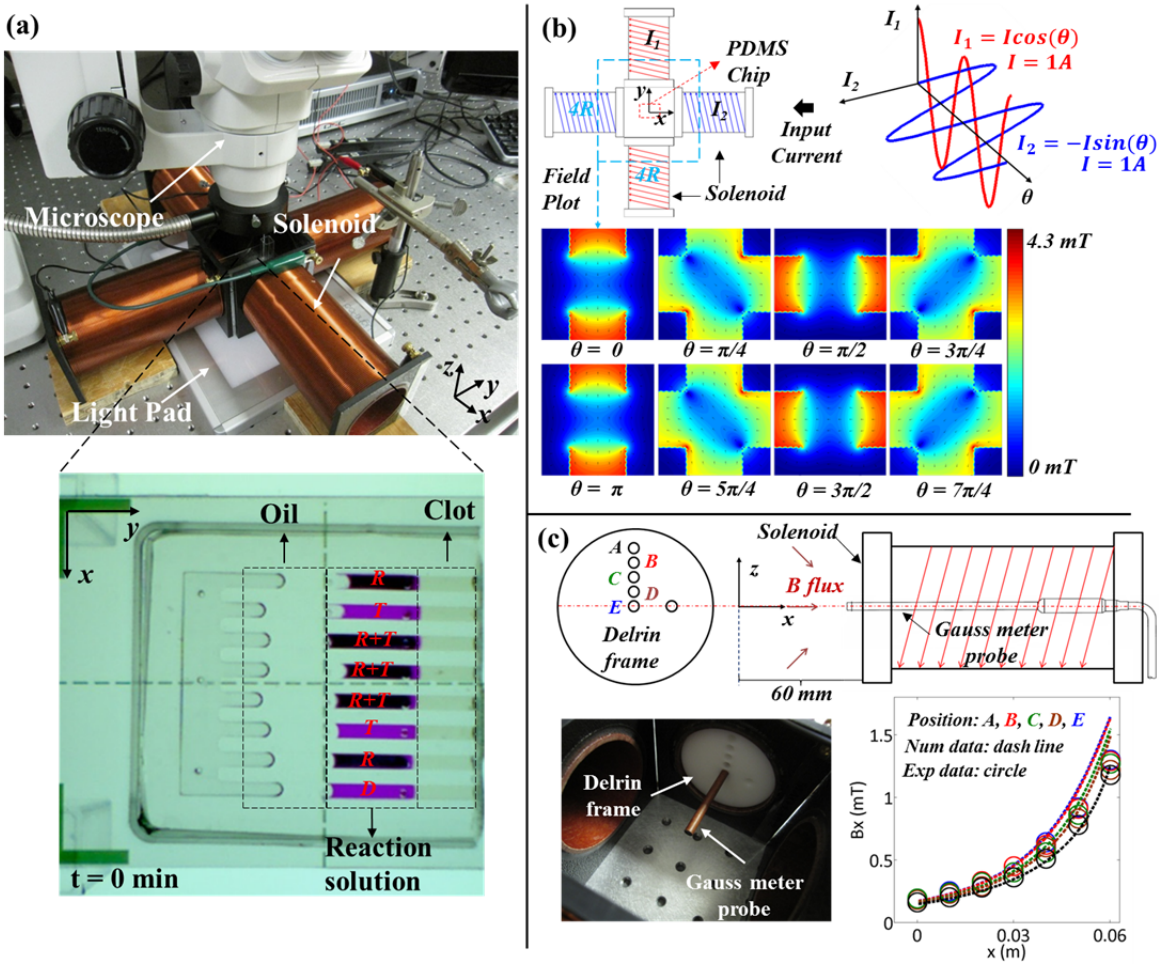

Figure S1 *In-vitro* experimental setup. **(a)** An image of the experimental setup consisting of the magnetic field generator, light pad, PDMS plate, and a microscope. **(b)** Numerical simulation of the rotating magnetic field in one cycle/period. **(c)** Experimental calibration of the magnetic field induced by a single solenoid.

Figure S1(b) shows the top view of the magnetic field generated by the solenoids, calculated by Biot-Savart law using Matlab (The MathWorks, Natick, MA). For the two pairs of solenoids, the input alternating currents have the same magnitude and frequency, but with a phasic lag of $\pi/2$. **Figure S1(b)** also depicts the magnetic field distribution within a 4R×4R blue-dash frame, where

R is the radius of the solenoid. From the field plots at different phase angle in one revolution, one can see the field is relatively uniform in the central area where the PDMS plate is placed. To verify the validity of the theoretical calculation, the field strength is measured to compare with the numerical field distribution. As shown in **Figure S1(c)**, a Gauss meter (Model 5080, F. W. BELL) probe through a homemade delrin frame embedded in a solenoid is used to measure the magnetic field strength in ***x*** direction at different locations, the theoretical prediction is consisted with the experimental data.

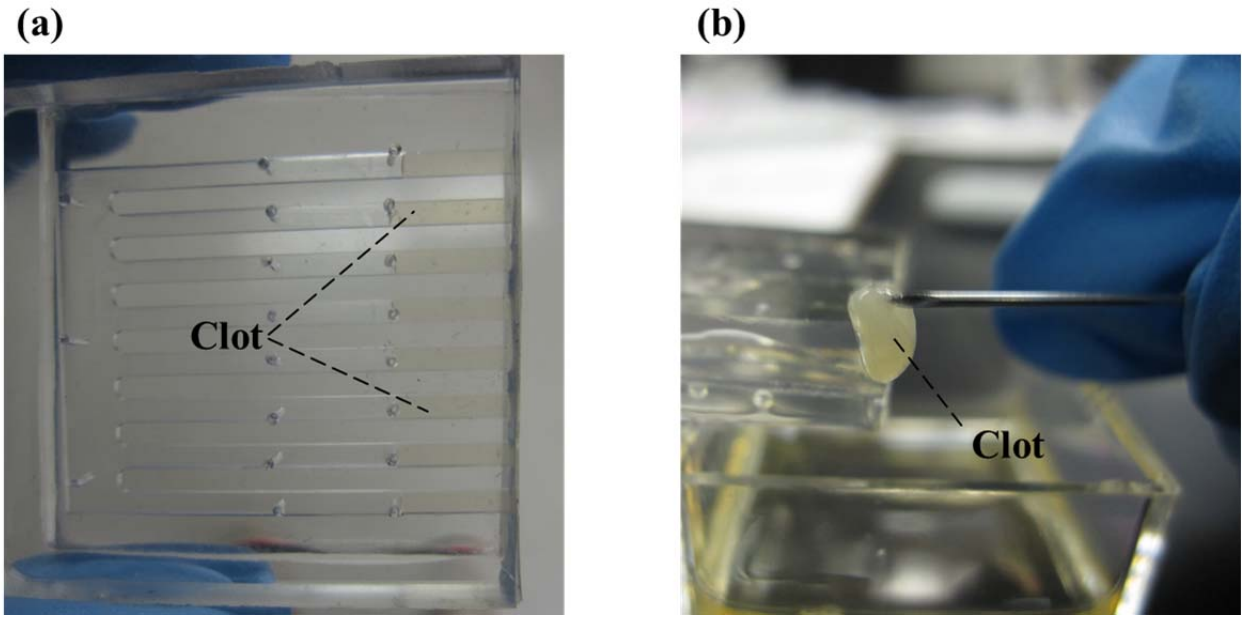

Figure S2 Fabricating clot inside PDMS channels. **(a)** PDMS channels plugged with clot, shown as light-yellow segments. **(b)** A clot pricked from a PDMS channel after fully reaction.

A novel method is developed to fabricate the length-controlled clot sections in PDMS channels. The clotting process is slowed down by mixing all the reagents at about 0℃, and the flow-able "clot" is injected into the PDMS channel to form uniform clot segments as described in the Experimental section in the main text. The light-yellow sections in the PDMS channels, as

shown in **Figure S2(a)**, are the clot segments. **Figure S2(b)** shows the tangled clot after it is removed from a channel after fully reacted.

1.2 In-vitro experimental data treatment method

The boundary moving is determined by the dye front moving in the PDMS channel. Since Rhodamine B (RDB) is a red colored dye, the grayscale in green color channel of the video image represents the RDB absorbance, which will depend on the RDB concentration and gives the best contrast, as shown in **Figure S3(a)** and **(b)**.

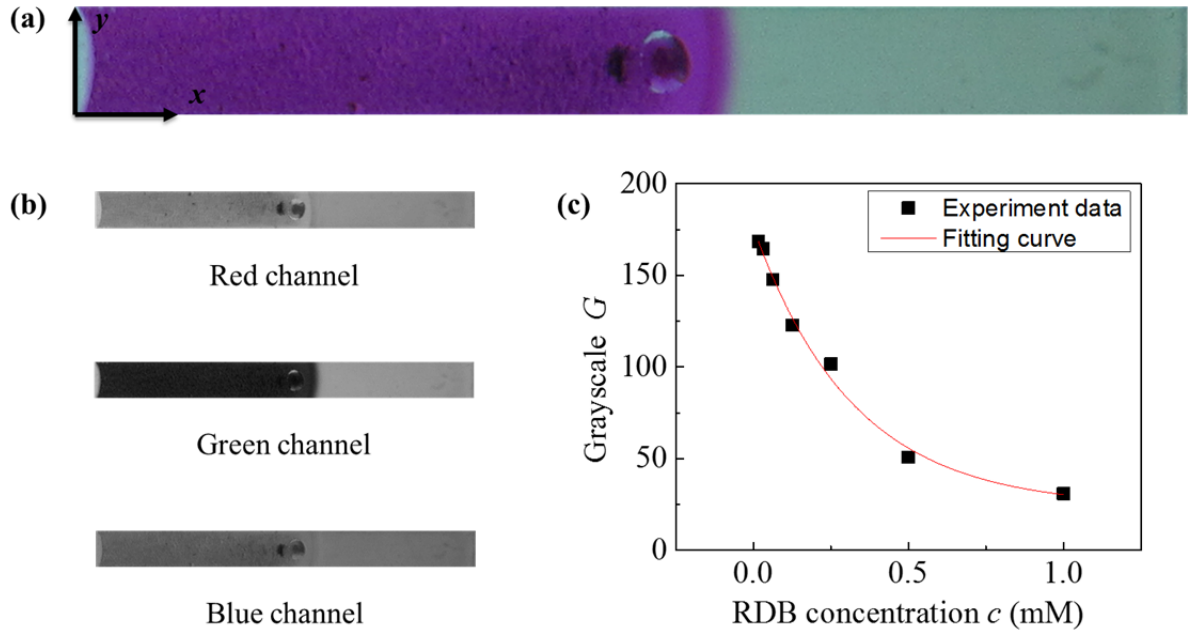

Figure S3 Data treatment process of *in-vitro* experiments. **(a)** Original image of a Dye+Rod channel at the beginning of the experiment with x-y coordinate definition. **(b)** The individual RGB color channel of the original image. **(c)** The calibration curve of the grayscale of the green channel *G vs.* RDB concentration *c*.

It is assumed that the transmitted green light intensity *I* follows Beer's Law,

$$\frac{I}{I_0} = e^{-\alpha l c} \quad , \tag{Eq.S1}$$

where I_0 is the incident green light intensity before the PDMS channel filled with RDB solution, c is the RDB concentration, α is the absorption coefficient, and l is the thickness of RDB solution, or the thickness of the channel. The grayscale of the image should be proportional to the transmitted light intensity,

$$\frac{G}{G_0} = \frac{I}{I_0} = e^{-\alpha l c} , \tag{Eq.S2}$$

where G and G_0 are the corresponding grayscale of the green channel of the video image. The calibration curve is shown in **Figure S3(c)**.

During the thrombolysis process, the grayscale value G of each channel is first averaged in y-direction,

$$G(x) = \frac{1}{h}\sum_{y} G(x, y), \tag{Eq.S3}$$

where h is the height of the image or channel width. Thus, G is a function of x coordinate only. The concentration of RDB is able to be estimated by,

$$c(x) = -\frac{1}{\alpha l}\ln\frac{G(x)}{G_0} . \tag{Eq.S4}$$

The boundary of the reaction solution and clot interface X_{boundary} is defined at where $\frac{dc}{dx}$ reaches the maximum value. The clot dissolving speed can be extracted by liner fitting of function $X_{\text{boundary}}(t)$ *vs.* time t.

To obtain the diffusion coefficient of RDB, the concentration curve at different time $c(x,t)$ is smoothened by averaging the five neighboring data points (5-point average) except at two boundaries,

$$c_{smooth}(x,t) = \frac{1}{5}\sum_{x-2}^{x+2} c(x,t) \ . \qquad \text{(Eq.S5)}$$

Since the solution of 1D diffusion equation $\frac{\partial c(\mathrm{x},\mathrm{t})}{\partial t} = D\frac{\partial^2 c(\mathrm{x},\mathrm{t})}{\partial x^2}$ is an error function:

$$c(x,t) = A\int_{\frac{x}{\sqrt{Dt}}}^{\infty} e^{-y^2} dy \ . \qquad \text{(Eq.S6)}$$

It indicates that the first derivative of c with respect to x will follow a Gaussian distribution,

$$\frac{\partial c(x,t)}{\partial x} = Ae^{-\frac{x^2}{Dt}} = Ae^{\frac{(x-\mu)^2}{\sigma^2}} \ . \qquad \text{(Eq.S7)}$$

Thus, the derivative $\frac{\partial c_{smooth}(x,t)}{\partial x}$ can be fitted by a Gaussian function, and the width of the Gauss function follows,

$$\sigma^2 = Dt \ . \qquad \text{(Eq.S8)}$$

Therefore, the diffusion constant D is obtained by liner fitting of σ^2 *vs.* time t.

1.3 In-vivo experimental setup

The rotational magnetic field employed for a rat embolic model is induced by permanent magnets. As schematically shown in **Figure S4(a)**, the device consists of two identical NdFeB magnets of rectangular shape (NdFeB, BY0X08DCS, K&J, Pipersville, PA), a homemade rotating frame and an AC motor (US560-001U2, Oriental Motor, Torrance, CA), of which the rotating speed can be continuously adjusted and digitally read from a indicator/controller

(SDM496, Oriental Motor, Torrance, CA). The permanent magnets are symmetrically mounted on the frame with their poles attractively facing each other. The rotating frame is made of aluminum and the mounting position is adjustable. Thus, the magnetic field distribution between the two magnets can be continuously adjusted for a designated value of local magnetic field strength at the infected hindlimb of rat (red-dash circle on rat paint).

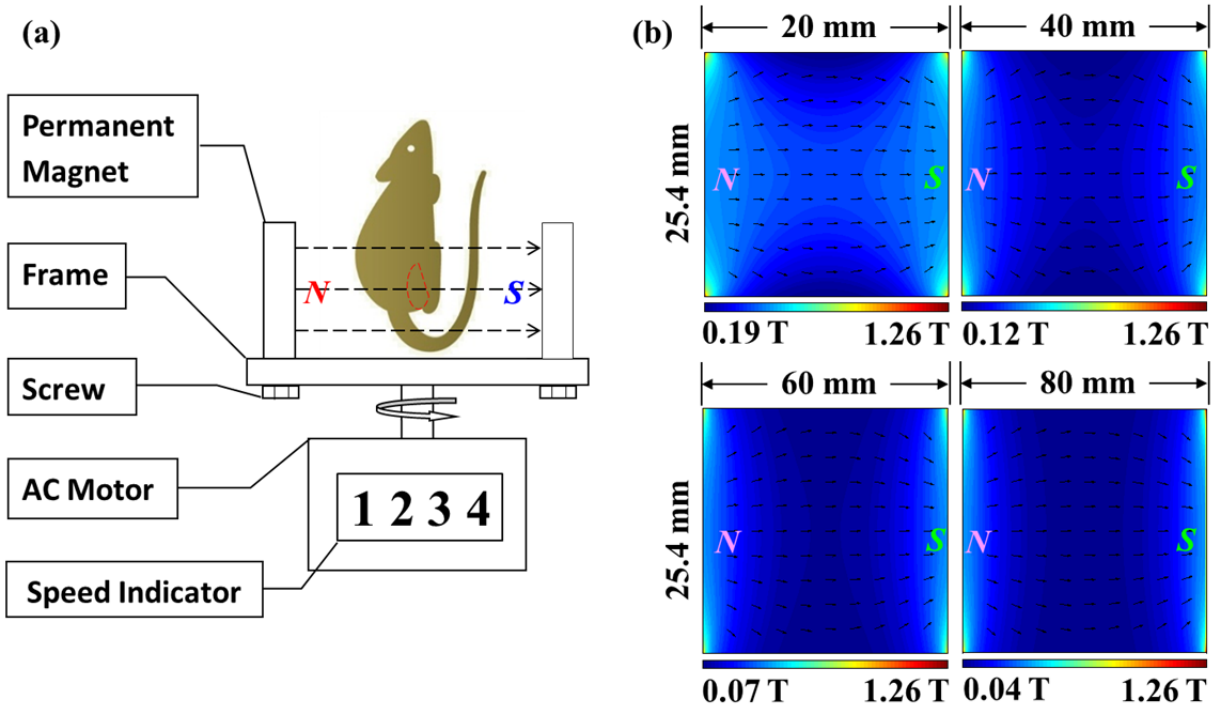

Figure S4 *In-vivo* experimental setup. **(a)** Schematic illustration of the apparatus. **(b)** Magnetic field distribution between two permanent magnets at different separations.

Figure S4(b) also plots four representative field distributions induced by the magnets in different locations. From the results, one can see the field strength is pretty uniform at the center of the magnet system. Its value varies from 40 mT to 200 mT, which satisfies the *in-vitro* experimental conditions.

2. Theoretical analysis on thrombolytic enhancement

2.1 Diffusion-controlled reaction of thrombolytic process

The clot remove process is a classic mass transport governing reaction process, and it could be simplified into 3 sub-process: (1) t-PA molecules (T) diffuse to the fibrin surface and bind onto fibrin lysine sites (S) to form t-PA-lysine complex (ST); (2) t-PA-lysine complex (ST) activates plasminogen into plasmin which cleaves fibrin into soluble product (P); (3) Product (P) desorbs from the fibrin surface and exposes new lysine sites, as proposed in **Figure 4(b)** in the manuscript and expressed in **Eq.S9**,

$$S + T \xrightarrow{k_T} ST \xrightarrow{k_{TP}} SP \xrightarrow{k_P} S + P \ . \qquad \text{(Eq.S9)}$$

Here, k_T is the adsorption rate of t-PA molecules on the fibrin surface and k_P is the desorption rate of product P removing from the fibrin surface. The process $ST \rightarrow SP$ involves multiple steps of bio-chemical reactions, and the intrinsic reaction rate is characterized by k_{TP}.

The thrombolysis rate is determined by how fast sub-processes (1) – (3) happen sequentially and is dominated by the slowest sub-process. For different concentration of t-PA, the overall thrombolysis could either belong to a diffusion limited reaction or a reaction limited process. The rate of diffusion limited reaction would depend closely on the t-PA bulk concentration, while a reaction limited process will be independent on the t-PA concentration, as well known in all chemical reaction systems. To confirm whether our current experiment condition (t-PA concentration = 50 μg/ml) belongs to a diffusion- or reaction- limited process, we have conducted a t-PA concentration dependent clot lysis speed experiment in the eight channels of our fluidic system, and the result is shown in the **Figure S5** below. From **Figure S5**, when $C_{tpa} \geq$ 200 μg/mL we can see the clot lysis speed v_T = 55 μm/min and it is saturated at higher C_{tpa}. At C_{tpa} = 50 μg/mL, the clot lysis speed v_T is about 35 μm/min and depends strongly on C_{tpa} , which

is a clear demonstration of diffusion limited process, *i.e.*, the transport (diffusion) of t-PA to the surface of clot is the slowest step to determine the overall reaction rate. Therefore, the t-PA molecular mobility or the diffusion coefficient can be enhanced through the rotating nanorods, and thus lead to enhanced reaction rate. Furthermore, the maxima clot lysis speed is limited at about 2 times as the speed at C_{tpa} = 50 μg/mL, which is consistent to the rod enhanced experiment.

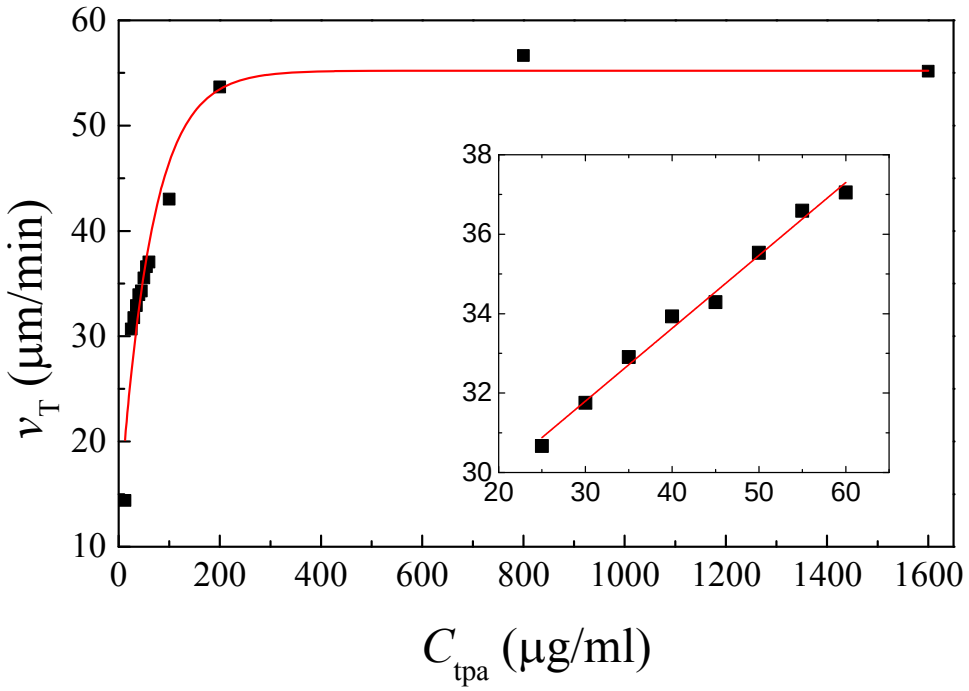

Figure S5 The clot boundary moving speed v_T *versus* the t-PA concentration C_{tpa}

2.2 Theoretical model of thrombolytic enhancement

As shown in **Eq.S9**, assuming the coverage of *ST* on the surface is Θ_1 while the coverage of *SP* is Θ_2, and the coverage for the vacant lysine sites should be 1- Θ_1- Θ_2. Then the rate equations for Θ_1 and Θ_2 can be expressed as,

$$\begin{cases} \dfrac{d\Theta_1}{dt} = k_T\left(1-\Theta_1-\Theta_2\right)-k_{TP}\Theta_1 \\ \dfrac{d\Theta_2}{dt} = k_{TP}\Theta_1 - k_P\Theta_2 \end{cases}, \qquad \text{(Eq.S10)}$$

The removal rate of product P with N_P available sites is,

$$\frac{dN_P}{dt} = k_P\Theta_2 . \qquad \text{(Eq.S11)}$$

Under equilibrium, **Eq.S10** gives,

$$\begin{cases} \Theta_1 = \dfrac{k_T k_P}{k_T k_{TP} + k_{TP}k_P + k_P k_T} \\ \Theta_2 = \dfrac{k_T k_{TP}}{k_T k_{TP} + k_{TP}k_P + k_P k_T} \end{cases}. \qquad \text{(Eq.S12)}$$

Combining **Eq.S11** and **Eq.S12**, we have,

$$\frac{dN_P}{dt} = \frac{k_T k_P k_{TP}}{k_T k_{TP} + k_{TP}k_P + k_P k_T} . \qquad \text{(Eq.S13)}$$

Eq.S13 shows that the thrombolysis speed is determined by the reaction coefficients of all three steps in the thrombolytic model of **Eq.S9**. According to the experimental observation, however, if we consider a diffusion limited process, i.e, $k_{TP} >> k_T$ and $k_P >> k_T$, **Eq.S13** reduces to,

$$\frac{dN_P}{dt} = k_T . \qquad \text{(Eq.S14)}$$

If every productive molecule P frees a volume V_P from solid clot by dissolving process, then the observed clot dissolving speed in our experiments can be expressed as,

$$v_{R+T} = \frac{V_P}{A_C\left(1-\Phi\right)}k_T , \qquad \text{(Eq.S15)}$$

where A_c is the cross-section area of the PDMS channel, Φ is the porosity of clot which can be assumed to be a constant.

According to the von Smoluchowski's equation, the classic result of conjugation rate k_T between t-PA molecules and lysine sites is given as[1],

$$k_T = 4\pi\left(D_{tpa} + D_{lysine}\right)\left(R_{tpa} + R_{lysine}\right)C_{tpa}\,, \qquad \text{(Eq.S16)}$$

where D_{tpa}, D_{lysine} represents the molecular diffusivities of t-PA and lysine site. R_{tpa}, R_{lysine} is the radius of t-PA molecules and lysine sites. C_{tpa} is the bulk t-PA concentration. Since the vacant lysine sites on clot surface are not moving, **Eq.S16** becomes,

$$k_T = 4\pi D_{tpa}\left(R_{tpa} + R_{site}\right)C_{tpa}\,. \qquad \text{(Eq.S17)}$$

From **Eq.S17**, the reaction rate k_T is proportional to the diffusivity D_{tpa} and the concentration C_{tpa} of t-PA molecules. With rotating rods induced flow field in our experiments, apparently, D_{tpa} contains two parts: thermally induced diffusion D_{tpa}^{T} and convectional flow enhanced diffusion by rotating rods D_{tpa}^{C} [2, 3],

$$D_{tpa} = D_{tpa}^{T} + D_{tpa}^{C}\,. \qquad \text{(Eq.S18)}$$

D_{tpa}^{T} can be estimated from Einstein's theory (see the result below), while the expression of D_{tpa}^{C} depends on the Peclet number Pe according to convection theory,

$$Pe = \frac{\overline{u}d_R}{D_{tpa}^{T}}\,, \qquad \text{(Eq.S19)}$$

where $\overline{u}$ is the average velocity of the flow field and $d_R = C_{NR}^{-1/3}$ is the size of each cellular flow induced by a rotating rod, confined in a cylindrical volume with height and diameter of d_R, as shown in **Fig. 3(b)** (for the convenience of derivation, C_{NR} is the number concentration of rods, which is different from the mass concentration of rod C_R defined in the manuscript). Due to the low speed and small size, the rotating rods are modeled as concentrated torques inducing Stokes' creeping flow at low Reynolds number. For a singular point torque $\vec{M}$ at the origin, the strength

of rotlet $\vec{\gamma}$ in a closed control surface is [4],

$$\vec{\gamma} = \frac{\vec{M}}{8\pi\eta} \ , \tag{Eq.S20}$$

where η is the viscosity of liquid.

While the velocity of a point on the surface positioning of vector $\vec{r}$ equals,

$$\vec{u} = \frac{\vec{\gamma} \times \vec{r}}{\left|\vec{r}\right|^3} \ , \tag{Eq.S21}$$

Thus, the velocity field induced by a rotating nanorod can be expressed as,

$$\vec{u} = \frac{\vec{M} \times \vec{r}}{8\pi\eta\left|\vec{r}\right|^3} \ , \tag{Eq.S22}$$

Obviously, the hydrodynamic volume by a single rod is cylindrically symmetric with induced velocity decaying as r^{-2}. If more than one rod are put in the liquid with a uniform distribution and applied by an equal driven torque M, the flow velocity by multi-rotating rods can be averagely estimated as,

$$\overline{u} = \frac{\sum_{i=1}^{n} \int_{\Omega_i} \left|\vec{u}\right| d\Omega}{V_L} = \frac{\left|\vec{M}\right| C_{NR}^{\ 2/3}}{4\eta} \ln\left(1+\sqrt{2}\right) \ , \tag{Eq.S23}$$

Here, $\Omega_i = \pi d_R^3 / 4$ is the hydrodynamic volume of a single rod, V_L is the total volume of the liquid. At the low Reynolds, the singular point torque $\left|\vec{M}\right|$ by a rotating nanorod equals to the hydrodynamic drag torque on it,

$$\vec{M} = 2\int_0^{L/2} (\vec{\mathrm{D}}_l \times \vec{l}) dl = \frac{-2\pi^2 \eta \varepsilon L^3 f}{3}, \tag{Eq.S24}$$

where $\vec{\mathrm{D}}_l = 4\pi\eta\varepsilon U(l)$ is the Lamb drag per unit length of rod[5], which is proportional to the distribution of flow velocity along the rod $U(l) = 2\pi fl$ and the shaped determined constant

$\varepsilon = \left(\ln\left(\frac{L}{d}\right) - 0.66 \right)^{-1}$ [6]. For a rod of length L = 1 μm and diameter d = 0.5 μm rotating at frequency f = 20 Hz, the induced torque $\vec{M} = 3.97 \times 10^{-18} N \cdot m$. With all known conditions, for example, when C_R = 7mg/mL, the highest concentration used in our experiments, the average hydrodynamic velocity induced by rotating rods $\bar{u}$ is about 11 μm/s; while C_R = 1mg/mL, $\bar{u} = 3$ μm/s. Since the diameter of t-PA soluble molecule is about 10 nm[7], the thermal diffusivity of t-PA molecules without rods can be estimated using Einstein's theory,

$$D_{tpa}^{T} = \frac{\kappa_B T}{6\pi\eta R_{tpa}} = 4.5 \times 10^{-11} m^2 / s, \qquad \text{(Eq.S25)}$$

where k_B, T and η are the Boltzmann constant, temperature, and viscosity of water, respectively. According to results of **Eq.S23**, with **Eq.S25**, we have Peclet number *Pe* in **Eq.S19** varies from 1.6 to 3.1 when C_R changes from 1 to 7 mg/ml in our experiments. When the Peclet number *Pe* is small (Pe<3)[2], the flow scaling law is valid for rigid-boundary conditions and the convectional flow enhanced diffusivity D_{tpa}^{C} in **Eq.S18** can be estimated as[3, 8],

$$D_{tpa}^{C} = aPe^2 D_{tpa}^{T}, \qquad \text{(Eq.S26)}$$

where a is a constant regarding to the flow field.

Combining **Eq.S15-Eq.S26**, the theoretical prediction of thrombolysis observed in our experiments shall obey the following relation with respect to nanorod concentration C_R,

$$v_{R+T} = v_T + \alpha C_R^{2/3}, \qquad \text{(Eq.S27)}$$

where, $v_T = \kappa C_{tpa} D_{tpa}^{T}$, where $\kappa = \frac{4\pi\left(R_{tpa} + R_{site}\right)V_P}{A_C\left(1-\Phi\right)}$, χ is a unit convertor so that $C_{NR} = \chi C_R$, and $\alpha = \kappa C_{tpa} \frac{0.0486 a \left|\vec{M}\right|^2 \chi^{2/3}}{\eta^2 D_{tpa}^{T}}$.

When C_R = 0, **Eq.S27** degrades to,

$$v_T = \kappa C_{tpa} D_{tpa}^T . \qquad \text{(Eq.S28)}$$

Here, the thrombolysis speed v_T (without rods) is proportional to C_{tpa}. This is true in the region of low concentration of t-PA, as shown in **Figure S5**. Obviously, C_{tpa} = 50 μg/ml for the rod enhanced thrombolysis is in the linear region of our experiments. Thus, the coefficient κD_{tpa}^T in **Eq.S28** can be extracted from the slop of the curve in the linear region in **Figure. S5**, as shown in the insert plot, and we obtain $\kappa D_{tpa}^T = 3.03\times10^{-6}$ $m^4\cdot kg^{-1}\cdot s^{-1}$. Since D_{tpa}^T is given by **Eq.S25**, we have $\kappa = 6.69\times10^4$ $m^2\cdot kg^{-1}$. In addition, the coefficient $a = 2/3\pi^2$ in the spatially periodic hydrodynamic flows[8], therefore,

$$\alpha = \kappa C_{tpa} \frac{0.0486a\left|\vec{M}\right|^2 \chi^{2/3}}{\eta^2 D_{tpa}^T} = 1.59\times10^{-4} ml\cdot mg^{-2/3}\cdot \min^{-1} . \qquad \text{(Eq.S29)}$$

Experimentally we obtain α = (9±2) × 10^{-4} ml $mg^{-2/3}$ min^{-1}, which is in the same order of magnitude estimated by the theory (**Eq.S19**). The discrepancy between the experimental value and the theoretical value could be due to the hydrodynamic effect of "rod cluster".

2.3 The effect of nanorods aggregation

The nanorods were treated by PVP to enhance the stability. When no external magnetic field applied, the rods of both low and high concentration suspended in the solution are uniformly distributed. However, it is observed they will form chain-like structures under a static external magnetic field. When the magnetic field is rotating, such chain structure will either maintain to rotate as "big rod" or break down into rods clusters as individual rotates[9]. We performed an experiment to test the cluster size of nanorod solution at different concentration under current experiment condition. If the cluster is not circular, the longest diameter will be used. **Figure S6** shows the average cluster size *versus* nanorod concentration for our experiments.

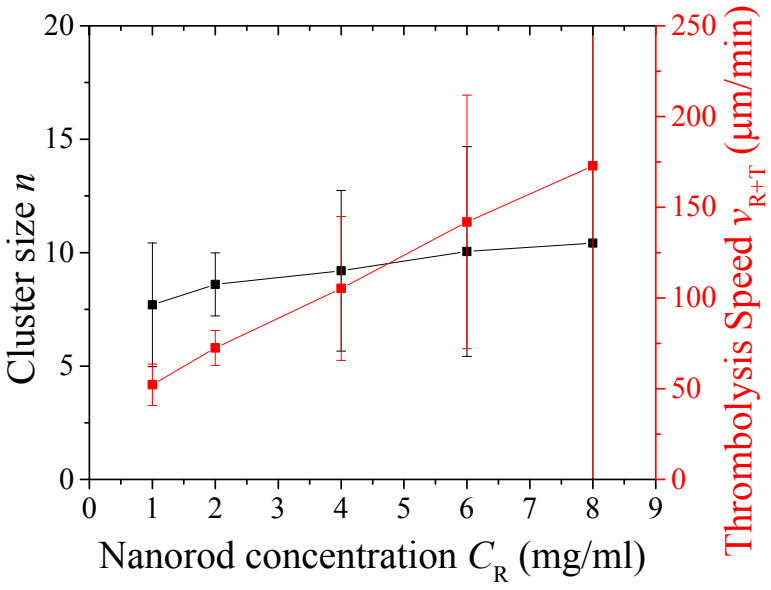

Figure S6 The cluster size distribution (black) and the theoretical prediction of the upper-bound thrombolysis with uncertainties (red) *versus* different rod concentration C_R

From the **Figure S6**, the average cluster size $n = C_{NR} / C_{cluster}$, defined the average number of rods in a cluster, and the uncertainty of the cluster size increases by the rods concentration. (Note that the error bar of cluster size n is up to ±17.28, and of theoretical thrombolysis speed v_{R+T} is up to ±327.51 μm/min at C_R = 8 mg/ml.) If each cluster can be treated as a rigid particle, **Eq.S27** can be modified as,

$$v_{R+T} - v_T = \Delta v = \alpha_{cluster} C_{cluster}^{2/3} = \kappa C_{tpa} \frac{0.0486a \left|\vec{M}\right|_{cluster}^2 C_{cluster}^{2/3}}{\eta^2 D_{tpa}^T}, \qquad \text{(Eq.S30)}$$

where $\left|\vec{M}\right|_{cluster}$ and C_{cluster} are the torque induced by a single cluster and the concentration of the torques, both of which depend on the cluster size. However, it is very difficult to estimate the magnitude of $\left|\vec{M}\right|_{cluster}$ using the hydrodynamic drag torque because the shape of the cluster varies location by location. On the other hand, even though we assume the driven torque induced by the magnetic field equals to the resistant torque by the hydrodynamic drag at the static rotation of a

cluster, the arrangement of rods in a cluster is unknown. Thus, we cannot simply employ the relation $\left|\vec{M}\right|_{cluster} = \sum \left|\vec{M}\right|_{rod}$ However, we know that,

$$\left|\vec{M}\right|_{cluster} \le n\left|\vec{M}\right|. \quad \text{(Eq.S31)}$$

Plug **Eq.S31** into **Eq.S30**, we have,

$$\Delta v \le \frac{0.0486 a\kappa C_{tpa}\left|\vec{M}\right|^2 C_{NR}^{2/3}}{\eta^2 D_{tpa}^T} n^{4/3} = \alpha' C_{NR}^{2/3}, \quad \text{(Eq.S32)}$$

where $\alpha' = \alpha n^{4/3}$ is the new proportionality of enhanced thrombolysis Δv with respect to $C_{NR}^{2/3}$ due to the presence of cluster. Then we can estimate the error bar of v_{R+T} using the uncertainty of rod-cluster size,

$$\delta v_{R+T} = \left|\frac{\partial \Delta v}{\partial n}\cdot \delta n\right| \le \frac{4}{3n}\alpha' C_{NR}^{2/3}\delta n. \quad \text{(Eq.S33)}$$

According to **Eq.S33** and **Figure S6**, the error bar of thrombolysis is predicted to increase by the rod concentration C_R, which is consistent to the trend of the experimental data in **Figure 3(d)**. Moreover, the term of $n^{4/3}$ in **Eq.S32** suggests the elevation of thrombolysis due to the hydrodynamic effect of clusters rather than rods.

2.4 The role of mechanical stimulation

The nanorods indeed have mechanical interaction with clot fiber. However, the force due to this interaction is too weak to break the clot fiber. Two evidences support this claim.

First, there is always a control channel only with nanorods in our experiments like channel R in **Figure 3(b**). In this channel, a lysis process can never been observed, instead, a diffusion process has always been observed as we reported in the manuscript (Page 6 Line 1). **Figure S7** shows the first derivative of dye concentration profile and the corresponding Gaussian fittings of *R* and *D* channels in **Figure 3(b)**. The parameter μ describes the central location of the Gaussian curve

and could be treated as the position of clot/dye diffusion boundary.

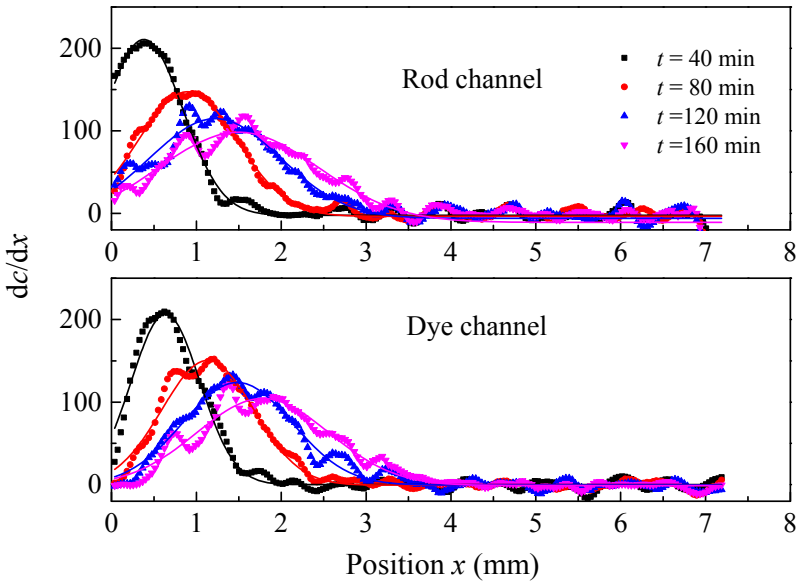

Figure S7 Change rate of dye concentration along the clot region

Figure S8 shows the plot of μ *vs.* t and simple liner fittings are given. According to **Figure S8,** the clot/dye boundary is moving in both D and R channels, and has almost the same speed (about 9 μm/min).

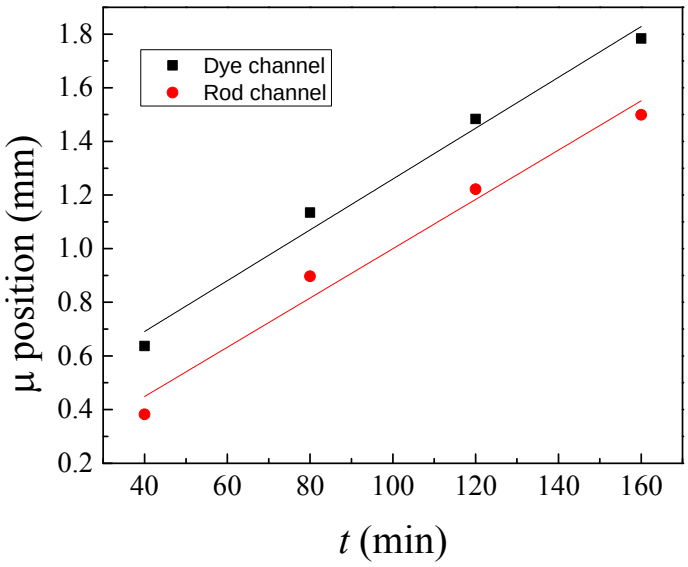

Figure S8 Plot of μ *vs.* t and liner fitting

This speed is coming from the staining process of clot since the clot is light yellow color and the stained clot appears a darker color than the dye solution. So the central location of the Gaussian curve will move accordingly. However, this does not mean that the clot is being dissolved. If the mechanical stimulation could enhance the clot lysis, we should expect a very different boundary moving speed in the *R* channel from in the *D* channel (a large slope in **Figure S8**), which is not the case in our observation.

Second, the mechanical force on a fibrin fiber by a rotating rod can be theoretically estimated. The Ni nanorod is modeled as a point-like magnet, as shown in **Figure S9**. Inside a uniform magnetic field, the magnet is subjected to a torque $\vec{T}$,

$$\vec{T} = \vec{m} \times \vec{B}, \qquad \text{(Eq.S34)}$$

where $\vec{m}$ is the dipole moment of the magnet, and $\vec{B}$ is the external magnetic flux. The torque is of the maximum magnitude when the dipole moment and the external magnetic flux are perpendicular to each other, and equal to zero when they are aligned with each other. The maximum torque, T_{max} is given by,

$$T_{\max} = mB, \qquad \text{(Eq.S35)}$$

where *m* and *B* are the magnitudes of the corresponding vectors.

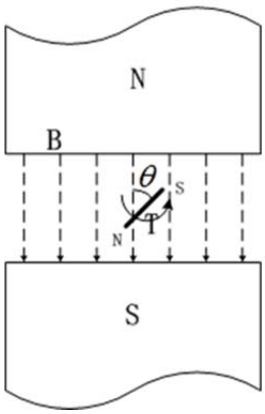

Figure S9: Schematic showing a magnet within a magnetic field.

Assuming that the Ni nanorods are magnetized along their longitudinal axes with magnetization M, the maximum torque is given by,

$$T_{\max} = MVB\,, \qquad \text{(Eq.S36)}$$

where V is the volume of the nanorod. The saturation magnetization of crystalline Ni is about 58.5 emu/g[10], and that of amorphous Ni is about one half of the value.[11] The mass density of Ni is 8900 kg/m^3. For a Ni nanorod with length l = 5 μm and diameter d = 0.2 μm, the volume, V = 0.157 μm^3. Let us assume B = 0.1 T, which is an overestimation in comparison to the field used in our experiments (B = 8 mT). Substituting all these parameters (note M set to be 32.9 emu/g for amorphous Ni) in **Eq.S36**, we can estimate T_{max} = 4.60 fN·m. It means that for the characteristic length scale down to the fibers of a fibrin clot, which should be ~ micron, such a nanorod/clot interaction can generate forces on the order of Nano Newton. On the other hand, according to the literature, it takes about 100 pN to unfold a fibril[12], and several thousands of parallel fibrils can be counted in a fiber cross section[13]. It means that it would take a force of ~ 1 μN to cause any damage to a fibrin fiber. As estimated above, the Ni nanorod can only exert a force about 1 nN. Thus, these nanorods cannot do any damage to individual fibers.

Therefore, from both experimental and theoretical analyses, we could conclude that the mechanical interaction between the magnetic nanorods and clot could hardly play an appreciable role in our present experiments of t-PA mediated thrombolysis.

References

1. Calef, D. F.; Deutch, J. Diffusion-Controlled Reactions. *Annual Review of Physical Chemistry* **1983,** 34, 493-524.

2. Mccarty, P.; Horsthemke, W. Effective Diffusion-Coefficient for Steady Two-Dimensional Convective Flow. *Phys. Rev. A* **1988,** 37, 2112-2117.

3. Rosenbluth, M. N.; Berk, H. L.; Doxas, I.; Horton, W. Effective Diffusion in Laminar Convective Flows. *Phys. Fluids* **1987,** 30, 2636-2647.

4. Chwang, A. T.; Wu, T. Y. T. Hydromechanics of Low-Reynolds-Number Flow .2. Singularity Method for Stokes Flows. *J. Fluid Mech.* **1975,** 67, 787-815.

5. Huner, B.; Hussey, R. G. Cylinder Drag at Low Reynolds-Number. *Phys. Fluids* **1977,** 20, 1211-1218.

6. Tirado, M. M.; Garciadelatorre, J. Rotational-Dynamics of Rigid, Symmetric Top Macromolecules - Application to Circular-Cylinders. *J. Chem. Phys.* **1980,** 73, 1986-1993.

7. De Vos AM, U. M., Kelley RF, Padmanabhan K, Tulinsky A, Westbrook ML, Kossiakoff AA. Crystal Structure of the Kringle 2 Domain of Tissue Plasminogen Activator at 2.4-Å Resolution. *Biochemistry (Mosc.)* **1992,** 31, 270-279.

8. Sagues, F.; Horsthemke, W. Diffusive Transport in Spatially Periodic Hydrodynamic Flows. *Phys. Rev. A* **1986,** 34, 4136-4143.

9. Petousis, I.; Homburg, E.; Derks, R.; Dietzel, A. Transient Behaviour of Magnetic Micro-Bead Chains Rotating in a Fluid by External Fields. *Lab Chip* **2007,** 7, 1746-51.

10. Danan, H. New Determinations of the Saturation Magnetization of Nickel and Iron. *J. Appl. Phys.* **1968,** 39, 669.

11. Rojo, J. M.; Hernando, A.; El Ghannami, M.; García-Escorial, A.; González, M. A.; García-Martínez, R.; Ricciarelli, L. Observation and Characterization of Ferromagnetic Amorphous Nickel. *Phys. Rev. Lett.* **1996,** 76, 4833-4836.

12. Brown André, E. X.; Litvinov, R. I.; Discher, D. E.; Weisel, J. W. Forced Unfolding of Coiled-Coils in Fibrinogen by Single-Molecule Afm. *Biophys J* **2007,** 92, L39-L41.

13. Collet, J. P.; Shuman, H.; Ledger, R. E.; Lee, S. T.; Weisel, J. W. The Elasticity of an Individual Fibrin Fiber in a Clot. *Proc. Natl. Acad. Sci. U. S. A.* **2005,** 102, 9133-9137.